Optics Communications 282 (2009) 360–366

Contents lists available at ScienceDirect

Optics Communications

journal homepage: www.elsevier.com/locate/optcom

Design of a solar concentrator combining paraboloidal and hyperbolic mirrors using ray tracing method

Chi-Feng Chen [a,b,*], Chih-Hao Lin [a], Huang-Tzung Jan [b,c], Yun-Ling Yang [a]

[a] Institute of Opto-Mechatronics Engineering, National Central University, Jhongli, Taiwan, ROC
[b] Department of Mechanical Engineering, National Central University, Jhongli, Taiwan, ROC
[c] Materials and Electro-Optics Research Division, Chung Shan Institute of Science and Technology, Tao-Yuan, Taiwan, ROC

ARTICLE INFO

Article history:
Received 7 May 2008
Received in revised form 6 October 2008
Accepted 10 October 2008

Keywords:
Solar energy
Solar concentrator
Two stage concentrator
Concentration
Concentrator tracing error
Ray tracing

ABSTRACT

A solar concentrator combining primary paraboloidal and secondary hyperboloidal mirrors is numerically designed by using the ray tracing method to obtain higher concentration ratio when the concentrator tracing error exists. It is found that, when the concentrator tracing errors are 0.5° or 1°, the concentration ratios are about 2027 or 1220 without the detector in the radial-direction, and the concentration ratios are about 5447 or 4701 with the detector in the radial-direction. It is shown that such method can increase the concentration solar flux by two folds when the concentrator tracing error exists. Obviously, it is an effective method to reduce the effect of concentrator tracing error even when the angle of concentrator tracing error is considered. In addition, when the angle of concentrator tracing error is small than 1°, a set of mirror shapes is suggested where the primary mirror has a *f*-number of 0.22 and the secondary mirror has a numerical aperture (NA) of 0.61.

1. Introduction

One of the most serious challenges facing us today is how to realize sustainable energy under the optimal balance of achieving social, economical and environmental sustainability. Sustainable energy becomes the main focus that people around the world are striving toward. An effective approach for sustainable energy is to deal properly with solar energy. Recently, many theoretical and experimental researches and commercial products focus on photovoltaic (PV) cell and solar heating [1–10]. One of the core researches is dedicated to producing photovoltaic cell with high conversion efficiency [7]. To meet this demand, an effective multi-junction cell technology was proposed to combine several semiconductor materials with differing bandgap energies. With the strong industry growth, such cells will soon achieve efficiencies in excess of 50%. The National Renewable Energy Laboratory (NREL) has been developing a concentrator triple-junction solar cell products forming by the compound semi combination of GaInP/GaAs/Ge thin films. This concentrator cells is current being shipped by Emcore to Green and Gold Energy of Glynde, Australia had demonstrated the current record conversion efficiency of 39% under high-concentration conditions (1000×) [8]. However, such high-efficiency PV cells are too expensive and complex to directly apply for commercial products.

To reduce the cost of the high-efficiency PV cells, the concentrating PV (CPV) systems combining a high-efficiency PV cell and a concentration system have been widely designed and proposed to concentrate the sunlight onto the cells [9–18]. Such concentration system is usually called concentrator. A parabola shaped trough reflector with the pipe being located at the focal point of the other parabola shaped reflector was disclosed [10]. When the water passes through the pipe, the water is then heated by the concentrated solar energy. To obtain maximum efficiency, the reflector is rotatable to fit the path of the sun. A new concept of concentrator for small paraboloidal dish array with low-attenuation optical fibers transporting power to a remote receiver was theoretically and experimentally explored [11–14]. This concentrator is a small paraboloidal dish with diameter of ~0.2 m. The sunlight is concentrated to the dish and transported to a remote receiver by a single optical fiber to be easily used for the applications. The result shows that the design of the maximum concentration fluxes are 30,000 suns (30 W/mm^2) [11]. A prototype with a diameter of 0.2 m is set up in Ref. [13]. The experimental results show that the flux of concentrated and transported sunlight propagating along a one-millimeter-diameter optical fiber up to 20 m away is 11,000–12,000 suns at a remote receiver. The other experimental system is presented and measured with

* Corresponding author. Address: Department of Mechanical Engineering, National Central University, Jhongli, Taiwan, ROC. Tel.: +886 3 4267308; fax: +886 3 4254501.
E-mail address: ccf@cc.ncu.edu.tw (C.-H. Lin).

0030-4018/$ - see front matter © 2008 Elsevier B.V. All rights reserved.
doi:10.1016/j.optcom.2008.10.017

deliverable power density up to 10^4 suns (10 W/mm^2), solar cell efficiencies above 30%, completely passive cooling, uniform and individualized cell illumination, and assembly from readily available components. The results show the feasibility of such designs to achieve a concentration level as high as thousands of suns [14]. A solar collector with Cassegrainian configuration was investigated for the storage of solar energy in a chemical system [15]. It is found that the focal length of the hyperboloid is not an important factor as long as it is similar to the focal length of the paraboloid. A two stage solar concentration with a paraboloidal dish primary mirror and a second-stage nonimaging concentrator was investigated and designed for high flux concentration at high collection efficiency [16]. For concentrators and illuminators, two stage reflector systems optical surface designed by aplanatic design technology were explored to provide radiative transfer at the thermodynamic limit [17]. The reflector shapes are analytically expressed by monotonic functions. Some practical results of the system with a wide range of numerical aperture for the application of solar concentration and light collimation are studied. A solar concentrator was disclosed to be used for concentrating sunlight with curved prismatic, Fresnel-type lens array being called stretched lens array [18–19]. Each of the prisms is arranged along the curve to convert the incident sunlight into a solar receiver. A stretched lens array consisted of a number of flexible line-focus Fresnel lenses with thickness of 140 μm, which was used to collect and focus sunlight at 8× concentration onto high-efficiency multi-junction photovoltaic cells [19]. The measurement result shows that net solar-to-electric conversion efficiency for space sunlight is over 27% and net solar-to-electric conversion is over 30%.

With the development of collectors and PV cells, the high-concentration collectors incorporated with high-efficiency cells are estimated by the Arizona Public Service to be the most cost-effective PV for commercial applications in the future. Furthermore, the concentrator is not only applied for photovoltaic but also for the thermal power generation [7–9], lighting systems [20], pumping of solar lasers [21], and solar thermochemical technology for high-efficiency Generation of hydrogen [22].

In this paper, we numerically investigate a solar concentrator combining primary paraboloidal and secondary hyperboloidal mirrors by using the ray tracing method to obtain higher concentration ratio. We establish a simulation tool of ray tracing and verify its accuracy by use Advanced Systems Analysis Program (ASAP™) which is developed by the Breault Research Organization. The simulation analysis is divided into two phases to effective find the optimal mirror shapes of such solar concentrator. Phase 1 is a preliminary analysis to quickly obtain a set of summary mirror shapes. Phase 2 is a detailed analysis based on the results of preliminary analysis and to reliably obtain the optimal mirror shapes. The designed results show that the concentration solar flux rapidly decreased with the concentrator tracing error (CTE). To solve the problem, we consider that the receiver is moving in the radial-direction. It has been proven that such method can increase the concentration solar flux by two folds when the CTE exists.

2. Simulation model

In this study, the solar concentrator combines the primary paraboloidal and secondary hyperboloidal mirrors. The sunlight propagates through the concentrator along the Z-direction, which is the optical axis of this system. The angels of ray deviated from optical axis are defined in the radial (R)-direction. Fig. 1 shows the schematic diagrams of (a) the module, (b) the sunlight distribution, (c) the primary paraboloidal part, and (d) the secondary hyperboloidal part for solar concentrator. F_1 and F_2 denote the foci

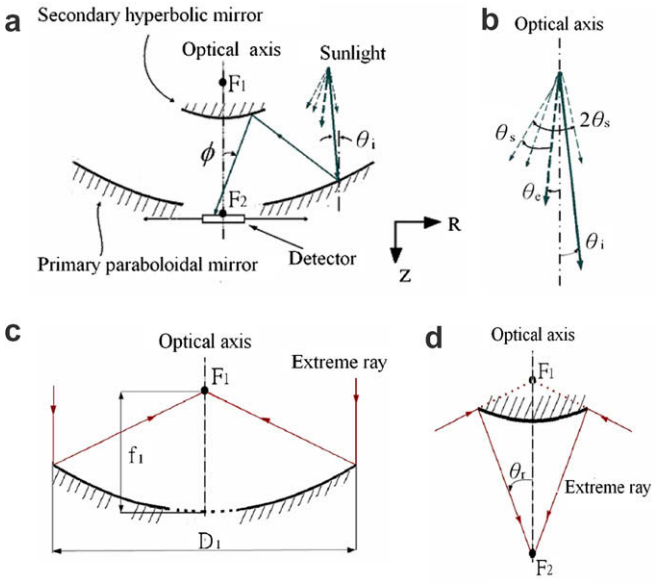

Fig. 1. Schematic diagrams of (a) the module, (b) the sunlight distribution, (c) the primary paraboloidal part, and (d) the secondary hyperboloidal part for solar concentrator combining primary paraboloidal and secondary hyperboloidal mirrors.

of the primary and secondary mirrors, respectively. θ_s and θ_e denote the half-angle of the inherent finite size of the sun and the angle of the CTE, respectively. θ_i and ϕ denote the angles of the incident ray and reflected ray at the second reflection, respectively. Here θ_s is considered 0.267° [23] and we ignore the other optical errors, such as misalignment, imperfect mirror contours, imperfect mirror specularity, etc. When the incident ray is parallel to the optical axis, the ray tracing of the extreme ray from the primary and secondary mirror's rims is shown in Fig. 1c and d where θ_r is the angle at which a ray reaches F_2. For this system, the position of the receiver (detector), such as PV cells, lens array, single fiber or fiber array, is at nearby F_2. To understand the effect of the geometric structure relations of two mirrors, we define f-number$_1$ for the primary mirror and NA$_2$ for the secondary mirror in the following.

$$f\text{-number}_1 = \frac{f_1}{D_1}, \tag{1}$$

$$\text{NA}_2 = \sin\theta_r \tag{2}$$

where f_1 is the focal length and is D_1 aperture diameter of the primary paraboloidal mirror. In this study, we consider that D_1 is equal to 1000 mm and F_2 is placed at 10 mm behind the apex of the primary mirror to conveniently set up a heat sink to cool the receiver, a device of receiving lights placed at the Z-axis position of F_2, or an actuator device to move the device of receiving lights in R-direction. In our numerical analysis, we use a detector to represent the device receiving lights and analyze its receiving solar flux. For the F_1 position correlated with the paraboloidal mirror, the schematic diagrams of three optical path types are (a) f-number$_1$ < 0.25, (b) f-number$_1$ = 0.25, and (c) f-number$_1$ > 0.25 shown in Fig. 2 when the different f-number$_1$ values are considered. Therefore, we choose f-number$_1$ = 0.15, 0.25 and 0.35 combining with the different NA$_2$ to come true our aim. The other mirror shapes, secondary aperture and distance between two apexes varied with NA$_2$ for the different f-number$_1$ are shown in Fig. 3. Here the distance between two apexes denotes the distance between the paraboloidal apex and hyperboloidal apex.

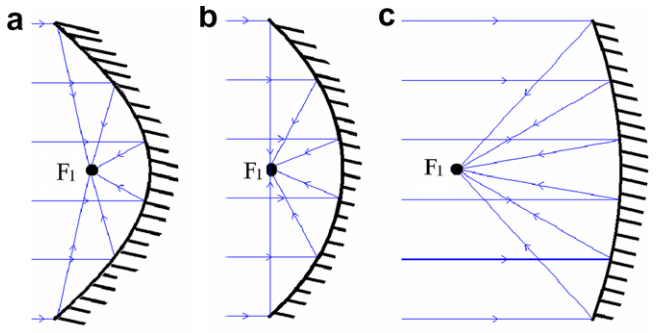

Fig. 2. Schematic diagrams of three optical path types when the different *f*-number$_1$ values are considered, (a) *f*-number$_1$ < 0.25, (b) *f*-number$_1$ = 0.25 and (c) *f*-number$_1$ > 0.25.

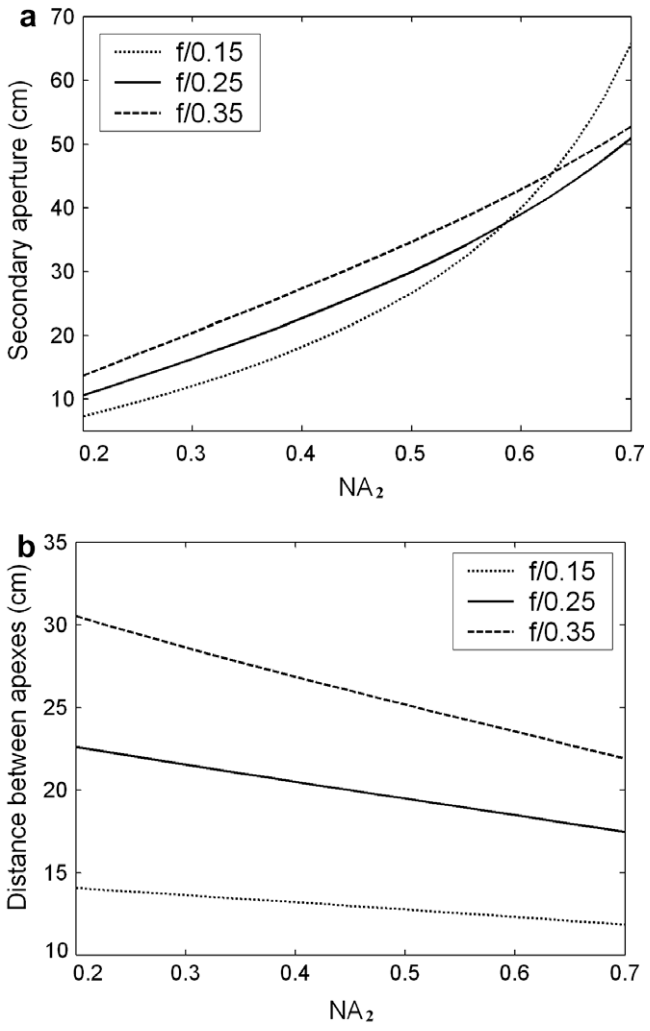

Fig. 3. Variances of (a) secondary aperture and (b) distance between two apexes with NA$_2$ for the different *f*-number$_1$.

In this paper, we use the concentration ratio (CTR) to judge the solar concentration effect and define as

$$\mathrm{CTR} \equiv \frac{\bar{H}_d}{\bar{H}_i} = \left(\frac{P_d}{P_i}\right) \cdot \left(\frac{A_i}{A_d}\right) = \eta_P \cdot \eta_A, \tag{3}$$

where $\bar{H}_i$ and $\bar{H}_d$ represent the average irradiances of initial incident concentration (primary paraboloidal mirror) and detector, η_P and η_A represent the ratios of the solar flux received by detector to the incident solar flux on primary paraboloidal mirror and the projection area of concentration to the detector area, A_i and A_d represent the projection area of concentration and the detector area, and P_i and P_d represent the solar flux received by detector and the incident solar flux on primary paraboloidal mirror, respectively. The size of detector is judged by the spot size of concentrated solar beam, that is, the detector radius is equal to the beam radius at which the intensity (irradiance) drop to $1/e^2$ of their maximum values.

Our simulation tool of ray tracing was self-established and verified by ASAP. The ASAP software based on the way that real light behaves in the real world is a very powerful tools to simulate optical system. Therefore, we regard the ASAP result as standard. Comparing two simulation results, the errors of spot size and CTR are always below 1% for all test samples. Here the errors are defined as

$$\mathrm{error}(\%) \equiv \left|\frac{\text{program result} - \text{ASAP result}}{\text{program result} + \text{ASAP result}}\right| * 100\%. \tag{4}$$

For example, when the *f-number*$_1$ is 0.25 and the CTE is ignored, the errors of (a) spot size and (b) CTR for the different NA$_2$ are shown in Fig. 4. One can see that the spot size and CTR errors are below 0.31% and 0.74%, respectively.

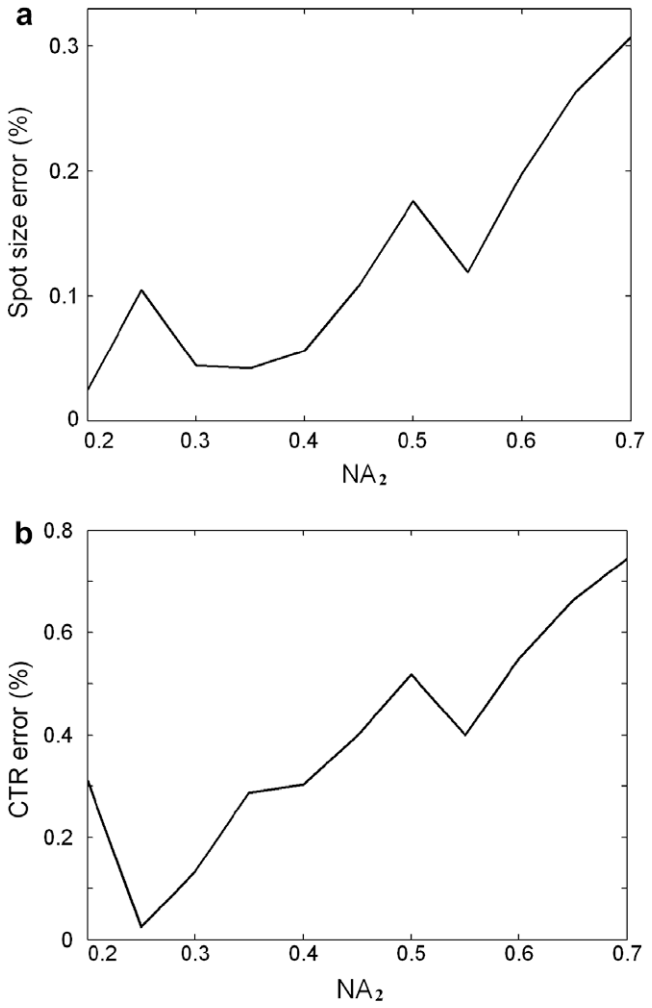

Fig. 4. Errors of (a) spot size and (b) CTR for the different NA$_2$ comparing two simulation results when the *f*-number$_1$ is 0.25 and the CTE is ignored.

3. Results and discussion

3.1. Preliminary analysis

3.1.1. Without CTE

First, we consider an ideal case where the CTE is ignored. The variances of (a) spot size and (b) CTR as a function of NA_2 for the different $f\text{-number}_1$ when $\theta_e = 0°$ are shown in Fig. 5. One can see that the spot sizes gradually become small with increasing NA_2 and the maxima of CTR can be found at $NA_2 = 0.59$, 0.62, and 0.64 for the cases where $f\text{-number}_1 = 0.15$, 0.25, and 0.35, respectively when the $\theta_e = 0°$. The total maximum of CTR is about 5889 at $f\text{-number}_1 = 0.25$ and $NA_2 = 0.62$. For all cases, the CTRs are above 5000 in the 0.48–0.66 NA_2 range. Comparing those results, it is found that the spot sizes and CTRs are more sensitive to NA_2 than $f\text{-number}_1$.

3.1.2. With CTE

Then, we investigate the effect of CTE for CTR. Fig. 6 shows the variances of (a) spot size, (b) CTR, and (c) spot position deviation from the optical axis in the radial-direction as a function of NA_2 for the different $f\text{-number}_1$ when $\theta_e = 0.5°$. It is seen from Fig. 6a that the spot sizes gradually become small with increasing NA_2 for all cases and the results are almost the same for two cases of $f\text{-number}_1 = 0.25$ and 0.35. From Fig. 6b, the CTRs gradually become large with increasing NA_2 when NA_2 is below 0.59, the maxima of CTR are obtain in theNA_2 range of 0.59–0.62 and the total maximum of CTR is about 2027 at the same without CTE condition. From Fig. 6c, the deviations gradually become small with increasing NA_2. When NA_2 is in the range of 0.40–0.65, the deviations are nearly the same for three cases. Fig. 7 shows the variances of (a) spot size, (b) CTR, and (c) spot position deviation from the optical

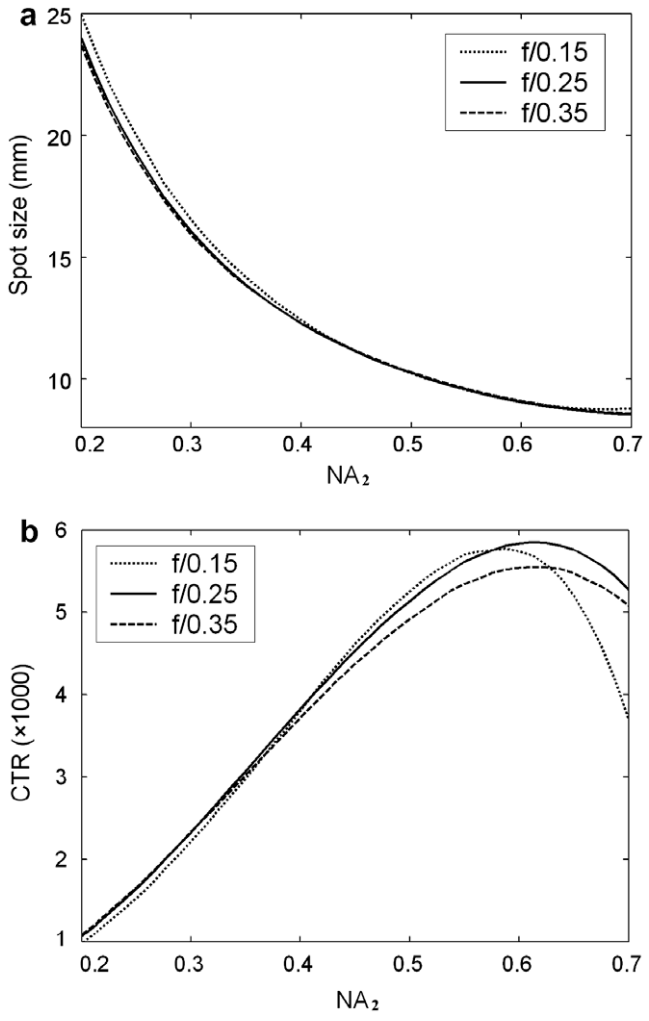

Fig. 5. Variances of (a) spot size and (b) CTR as a function of NA_2 for the different $f\text{-number}_1$ when $\theta_e = 0°$.

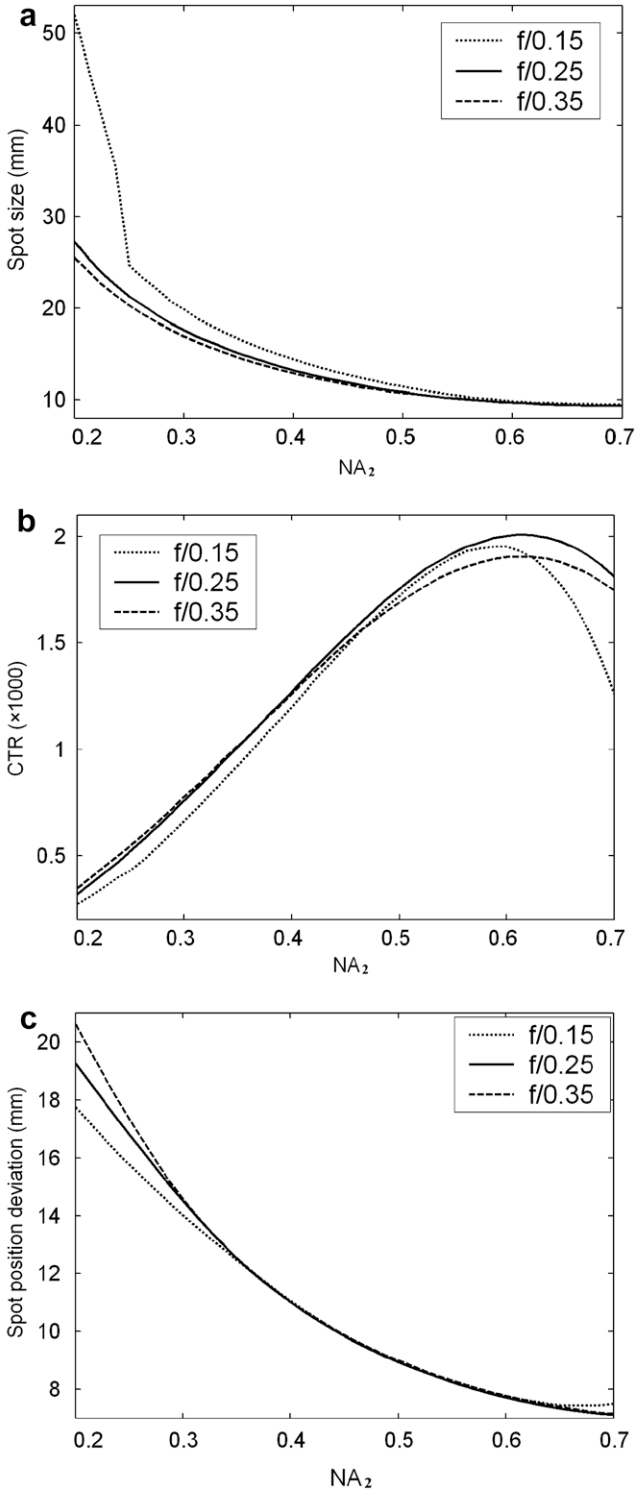

Fig. 6. Variances of (a) spot size, (b) CTR, and (c) spot position deviation from the optical axis in the *R*-direction as a function of NA_2 for the different $f\text{-number}_1$ when $\theta_e = 0.5°$.

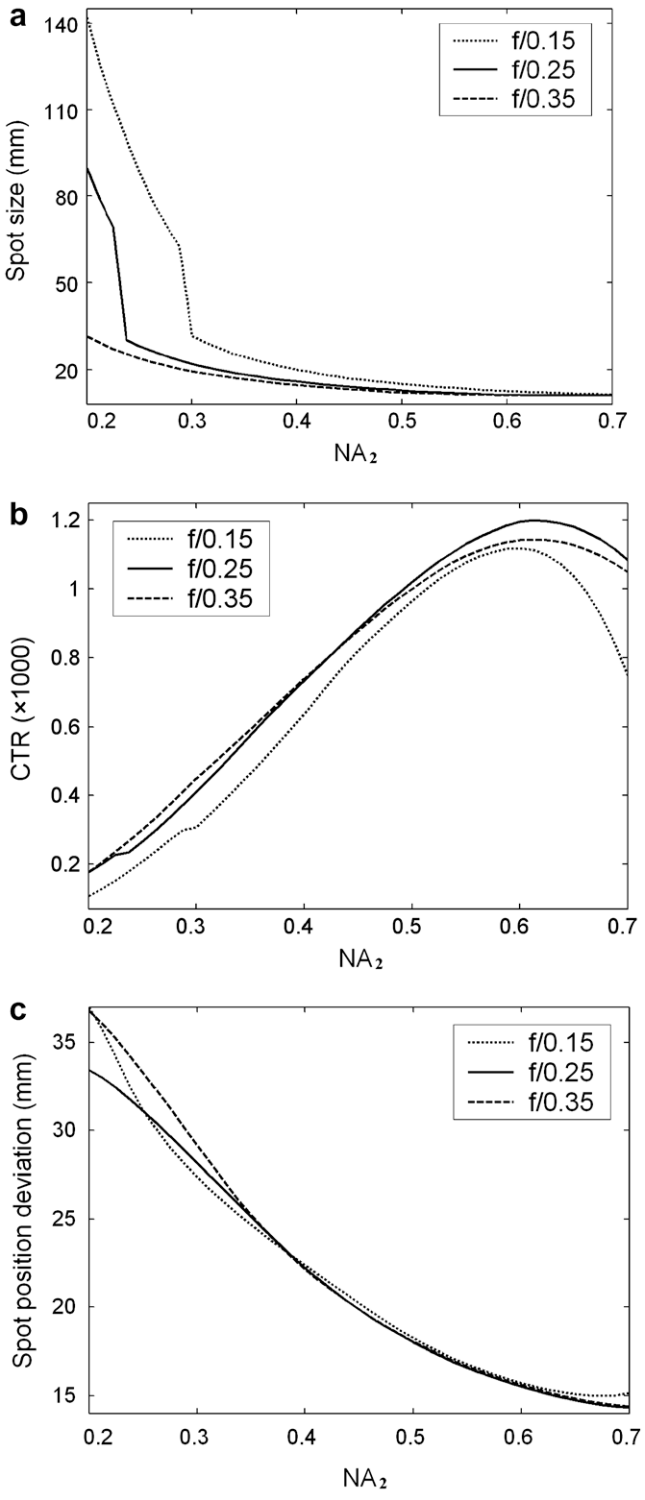

Fig. 7. Variances of (a) spot size, (b) CTR, and (c) spot position deviation from the optical axis in the *R*-direction as a function of NA_2 for the different *f*-number$_1$ when $\theta_e = 1°$.

axis in the *R*-direction as a function of NA_2 for the different *f-number*$_1$ when $\theta_e = 1°$. One can see that the variance tendencies of Fig. 7 are the same Fig. 6. The total maximum of CTR is obtained under the same condition, but the value goes down 1220. Obvious, when the CTE is considered, the spot sizes become big and the spot position deviation is generated. To concentrate the deviation and bigger spots, the detector fixed at F_2 must become enough large. It

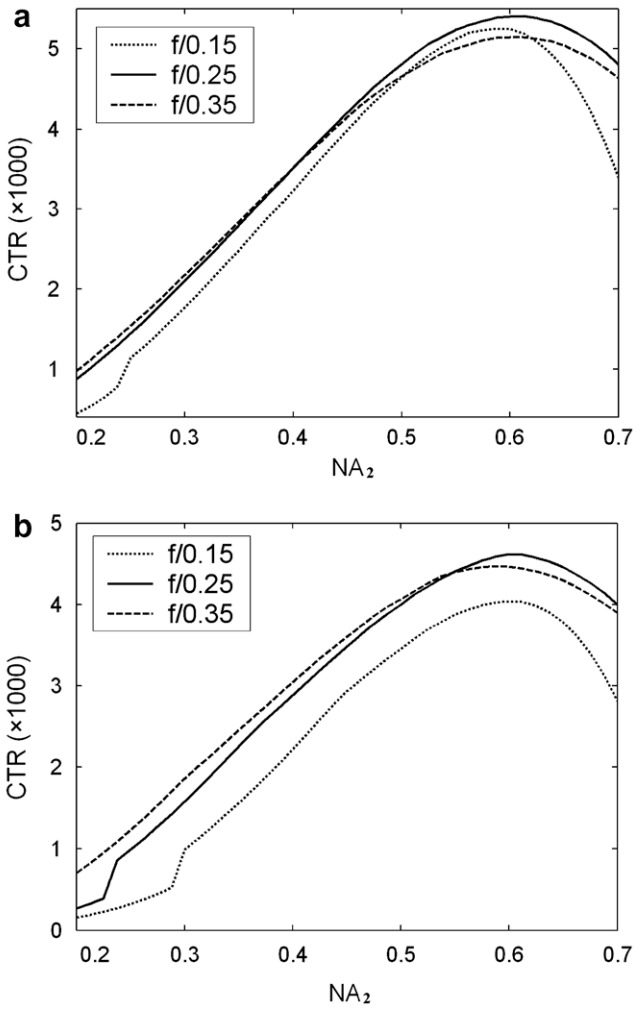

Fig. 8. Variances of (a) $\theta_e = 0.5°$ and (b) $\theta_e = 1°$ CTRs as a function of NA_2 the different *f*-number$_1$ when the detector is moved to the position of spot size deviation in the *R*-direction.

stands to reason that the value of CTR rapidly decrease when the CTE is existed.

3.1.3. Moving the detector in R-direction

To improve the problem that the CTR rapidly decrease when the CTE exists, we consider moving the detector in *R*-direction. Fig. 8 shows the variances of CTRs of (a) $\theta_e = 0.5°$ and (b) $\theta_e = 1°$ as a function of NA_2 for the different *f-number*$_1$ when the detector is moved to the position of spot size deviation in the *R*-direction. It can be seen that the CTRs comparing with Figs. 6c and 7c obvi-

Table 1
The maxima of CTR atNA_2 for the different *f*-number$_1$ without/with moving the detector in the *R*-direction.

CTE angle	Moving the detector	Maxima of CTR at NA_2 (Max. CTR @ NA_2)		
		f/0.15	*f*/0.25	*f*/0.35
0°	Without	5779 @ 0.59	5889 @ 0.62	5549 @ 0.64
0.5°	Without	1952 @ 0.59	2027 @ 0.62	1956 @ 0.61
	With	5251 @ 0.58	5447 @ 0.61	5142 @ 0.61
1°	Without	1118 @ 0.60	1220 @ 0.62	1144 @ 0.61
	With	4040 @ 0.60	4701 @ 0.60	4401 @ 0.59

ous increase over two times. From Fig. 8a, the CTRs are above 4500 in the 0.48–0.66 NA_2 range for all cases and the CTRs are above 5000 in the 0.53–0.68 NA_2 range for $f\text{-number}_1$ 0.25 case. The maxima of CTR can be found at $NA_2 = 0.58$, 0.6, and 0.61 for the cases of $f\text{-number}_1 = 0.15$, 0.25, and 0.35 when the $\theta_e = 0.5°$, respectively. From Fig. 8b, the CTRs are above 4000 in the 0.50–0.69 NA_2 range except for $f\text{-number}_1$ 0.15 case. The maxima of CTR can be found at $NA_2 = 0.6$, 0.6, and 0.59 for the cases of $f\text{-number}_1 = 0.15$, 0.25, and 0.35 when the $\theta_e = 1°$, respectively. The total maximum of CTR is about 5447 at $f\text{-number}_1 = 0.25$ and $NA_2 = 0.61$ and 4701 at $f\text{-number}_1 = 0.25$ and $NA_2 = 0.6$ when the $\theta_e = 0.5°$ and $\theta_e = 1°$. Apparently, it is an effective method to im-

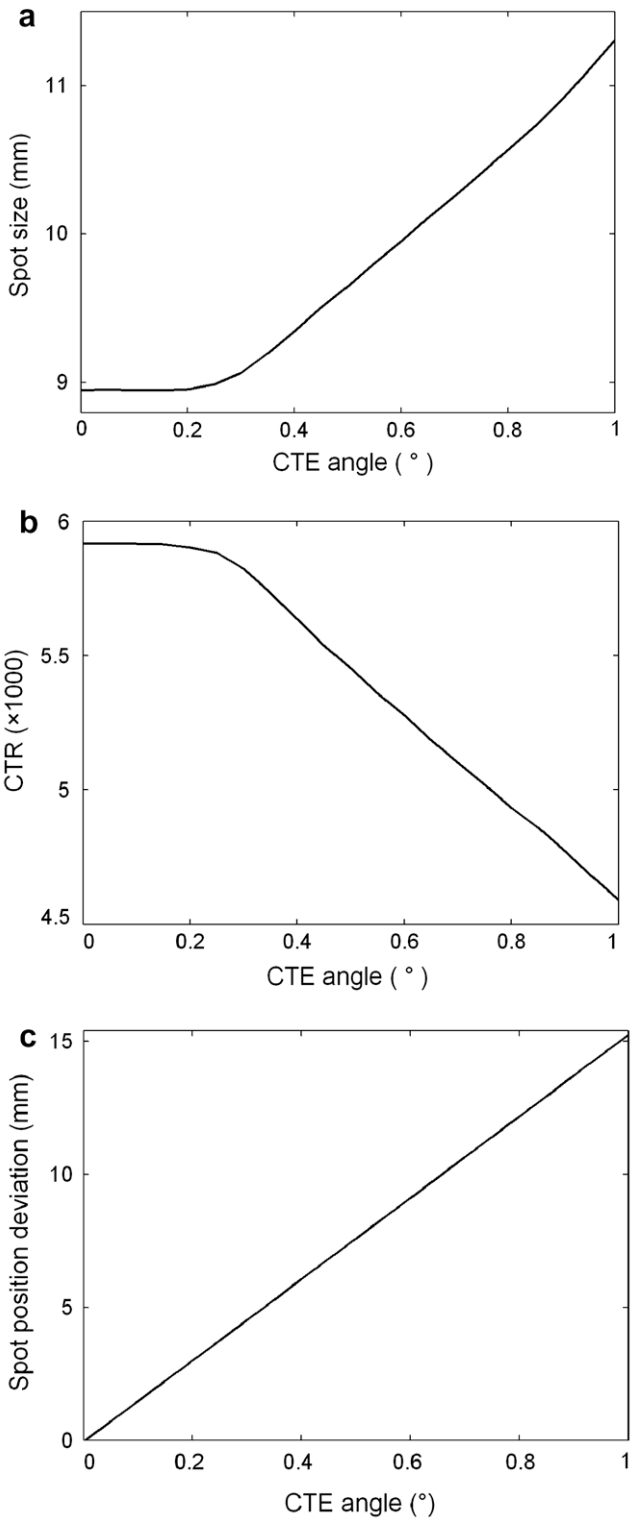

Fig. 9. Relations of (a) spot size, (b) CTR, and (c) spot position deviation with CTE angle for $f\text{-number}_1 = 0.22$ and $NA_2 = 0.61$.

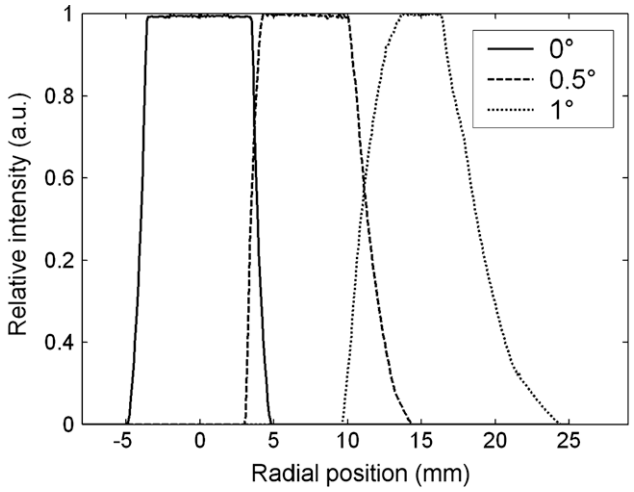

Fig. 10. Relative intensity distribution in the R-direction for the different CTE angle when $f\text{-number}_1 = 0.22$ and $NA_2 = 0.61$.

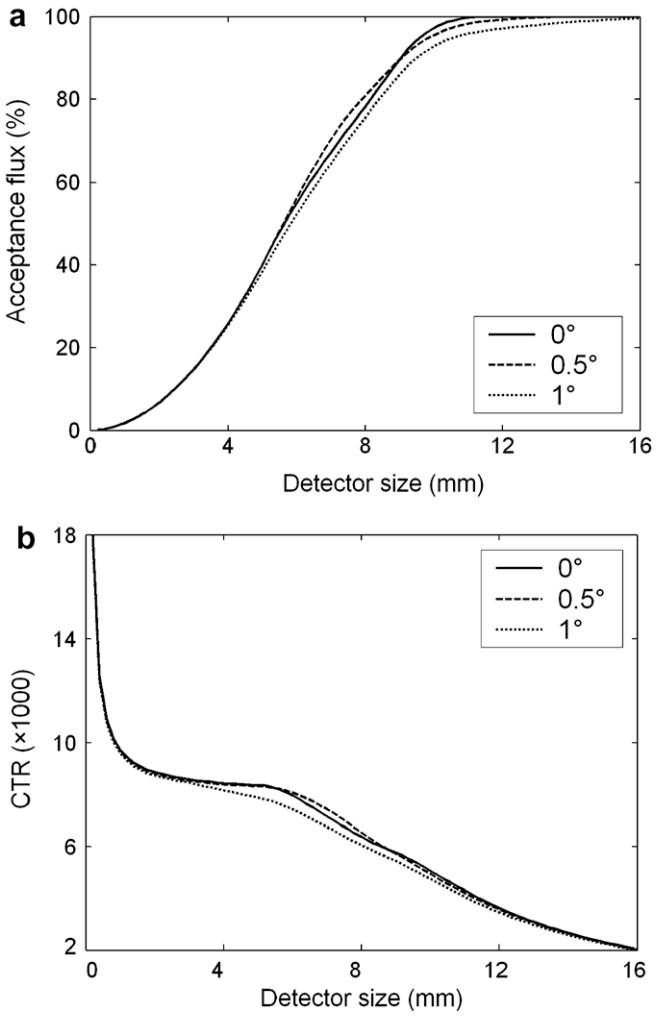

Fig. 11. (a) Acceptance flux and (b) CTR with the detector size for $f\text{-number}_1 = 0.22$ and $NA_2 = 0.61$.

prove the CTR. he detail results of the maxima of CTR atNA_2 or the different $f\text{-}number_1$ without/with moving the detector in the R-direction are listed in Table 1.

3.2. Advanced analysis

Based on the results of preliminary analysis, we further analyze in detail all mirror shapes when the CTE is considered. First, we take $f\text{-}number_1$ between 0.15 and 0.35, NA_2 between 0.5 and 0.7, and CTE angle between 0° and 1° to find a suitable mirror shapes of solar concentrator with higher CTR. Comparing those results, the parameters $f\text{-}number_1 = 0.22$ and $NA_2 = 0.61$ are chosen. Then, we further study the relations between these parameters and their effect for CTR.

The relations of (a) spot size, (b) CTR, and (c) spot position deviation with CTE angle are shown in Fig. 9. One can see that two curves have an obvious turning at CTE angle 0.25° for the spot size and CTR cases and the curve is close to linear and its slope is about 15.25 mm/° for the spot position deviation case. When CTE angle is below 0.25°, the spot size and CTR are almost steady equal to 8.99 mm and 5882, respectively. When CTE angle is over 0.25°, the spot size gradually becomes big with increasing CTE angle, its slope is about 3.20 mm/°, and the CTR gradually becomes small with increasing CTE angle, its slope is about -1758 degree^{-1}.

For an ideal concept, all solar flux is expected to be concentrated in the receiving device (detector). It is incompatible with the aim of high-concentration, because the area of receiving device is constant. If we wish to concentrate the greater part solar flux, the area of receiving device must be enough large when CTE is considered. It will lead to reduce CTR. The relative intensity distributions in the radial-direction for the different CTE angle when $f\text{-}number_1 = 0.22$ and$NA_2 = 0.61$ are shown in Fig. 10. Then, we try to change the detector size to understand the acceptance flux and CTR for the same as Fig. 9, the results are shown in Fig. 11. One can see that the CTRs are over 10,000 for all cases when the detector size is only 1 mm. But, the acceptance fluxes of detector are only 1.25%. If the acceptance fluxes of detector are 50%, CTRs are about 8201, 8213, and 7539 at detector sizes 5.6, 5.6, and 5.8 mm when $\theta_e = 0°$, 0.5°, and 1°, respectively.

4. Conclusion

In this paper, a solar concentrator combining primary paraboloidal and secondary hyperboloidal mirrors is investigated by using the ray tracing method to obtain higher concentration ratio. A simulation tool of ray tracing is established and verified its accuracy by ASAP™ software. The designed results show that the maxima of CTR are about 5889, 2027, and 1220 at f-number$_1 = 0.25$ and $NA_2 = 0.62$ for the CTE angles 0°, 0.5°, and 1° when the detector is fixed, respectively. If the receiver is moved to fit the spot position in R-direction, the maxima of CTR are 5447 and 4701 for the suitable mirror shapes when the CTE angles are 0.5° and 1°, respectively. On the whole, the optimal geometric structure relations, f-number$_1 = 0.22$ and$NA_2 = 0.61$, are obtained when the CTE angle $\leqq 1°$. It is shown that such method can increase the concentration solar flux over two times when the CTE is existed. Obviously, it is an effective method to reduce the effect of CTE.

Acknowledgement

This work is partially supported by National Science Council, Republic of China, under Contract NSC 96-2622-E-008-006-CC3.

References

[1] F. Lasnier, T.G. Ang, Photovoltaic Engineering Handbook, CRC Press, 1990.
[2] G. Yu, J. Gao, J.C. Hummelen, F. Wudl, A.J. Heeger, Science 270 (1995) 1789.
[3] L. Schmidt-Mende, A. Fechtenkötter, K. Müllen, E. Moons, R.H. Friend, J.D. MacKenzie, Science 293 (2001) 1119.
[4] R.M. Swanson, in: A. Luque, S. Hegedus (Eds.), Handbook of Photovoltaic Science and Engineering, J. Wiley & Sons, New York, 2003.
[5] N.S. Lewis, Science 315 (2007) 798.
[6] D.Y. Goswami, F. Kreith, J.F. Kreider, Principles of Solar Engineering, second ed., Taylor & Francis Publishers, London, 2000.
[7] M. Yamaguchi, T. Takamoto, K. Araki, N. Ekins-Daukes, Sol. Energy 79 (2005) 78.
[8] CompoundSemi News, September 4, 2007, <http://www.compoundsemi.com/documents/articles/news/8848.html>.
[9] S.A. Kalogirou, Prog. Energy Combust. Sci. 30 (2004) 231.
[10] Earl R. Hurkett, Solar Concentrator United States Patent 4,011,858.
[11] D. Feuermann, J.M. Gordon, Sol. Energy 65 (3) (1999) 159.
[12] D. Feuermann, J.M. Gordin, Sol. Energy 70 (2001) 423.
[13] D. Feuermann, J.M. Gordin, M. Huleihil, Sol. Energy 72 (2002) 459, Erratum 73 (2002) 73.
[14] J.M. Gordin, E.A. Katz, D. Feuermann, M. Huleihil, Appl. Phys. Lett. 84 (2004) 3642.
[15] C.E. Mauk, H.W. Prengle, C.H.S. Eddy, Sol. Energy 23 (1979) 157.
[16] D. Feuermann, J.M. Gordin, H. Ries, Sol. Energy 65 (1999) 83.
[17] J.M. Gordin, D. Feuermann, Appl. Opt. 44 (2005) 2327.
[18] M.J. O'Neill, Solar Concentrator and Energy Collection System United States Patent 4,069,812.
[19] M.J. O'Neill et al., SPIE's 48th Annual Meeting, San Diego, August 3–8, 2003 – Paper No. 5179-17.
[20] G.O. Schlegel, F.W. Burkholder, S.A. Klein, W.A. Beckman, B.D. Wood, J.D. Muhs, Sol. Energy 76 (4) (2004) 359.
[21] D. Liang, L.F. Monteiro, M.R. Texeira, M.L.F. Monteiro, M. Collares-Pereira, Sol. Energy Mater. Sol. Cells 54 (1998) 323.
[22] A. Steinfeld, Int. J. Hydrogen Energy 27 (2002) 611.
[23] J.A. Duffie, W.A. Beckman, Sol. Eng. Therm. Processes, Wiley-Interscience, New York, 1991.